

TERRESTRIAL ECOSYSTEM PRODUCTION: A  
PROCESS MODEL BASED ON GLOBAL  
SATELLITE AND SURFACE DATA

Christopher S. Potter,<sup>1</sup> James T. Randerson,<sup>2</sup>  
Christopher B. Field,<sup>2</sup> Pamela A. Matson,<sup>3</sup> Peter M.  
Vitousek,<sup>4</sup> Harold A. Mooney,<sup>4</sup> and Steven A.  
Klooster<sup>1</sup>

*Abstract.* This paper presents a modeling approach aimed at seasonal resolution of global climatic and edaphic controls on patterns of terrestrial ecosystem production and soil microbial respiration. We use satellite imagery (Advanced Very High Resolution Radiometer and International Satellite Cloud Climatology Project solar radiation), along with historical climate (monthly temperature and precipitation) and soil attributes (texture, C and N contents) from global (1°) data sets as model inputs. The Carnegie-Ames-Stanford approach (CASA) Biosphere model runs on a monthly time interval to simulate seasonal patterns in net plant carbon fixation, biomass and nutrient allocation, litterfall, soil nitrogen mineralization, and microbial CO<sub>2</sub> production. The model estimate of global terrestrial net primary production is 48 Pg C yr<sup>-1</sup> with a maximum light use efficiency of 0.39 g C MJ<sup>-1</sup> PAR. Over 70% of terrestrial net production takes

place between 30° N and 30° S latitude. Steady state pools of standing litter represent global storage of around 174 Pg C (94 and 80 Pg C in nonwoody and woody pools, respectively), whereas the pool of soil C in the top 0.3 m that is turning over on decadal time scales comprises 300 Pg C. Seasonal variations in atmospheric CO<sub>2</sub> concentrations from three stations in the Geophysical Monitoring for Climate Change Flask Sampling Network correlate significantly with estimated net ecosystem production values averaged over 50°-80° N, 10°-30° N, and 0°-10° N.

INTRODUCTION

The amount of carbon fixed annually via terrestrial net primary productivity (NPP) or released by soil microbial respiration ( $R_s$ ) is about an order of magnitude greater than the annual increase in atmospheric carbon dioxide (CO<sub>2</sub>) levels due to fossil fuel combustion [Ajtay, 1979; Houghton et al., 1992]. Seasonal changes in the balance between photosynthetic carbon fixation by land plants and microbial respiration are of a size sufficient to drive the intra-annual oscillation of atmospheric CO<sub>2</sub> concentration [Bacastow et al., 1985; Houghton, 1987]. Either carbon fixation or respiration could be affected substantially by components of global change (e.g., warming or elevated CO<sub>2</sub> concentrations), which raises the possibility of long-term modifications in the carbon balance of terrestrial ecosystems [Rastetter et al., 1991; Mooney et al., 1991] and feedbacks to global biogeochemistry and radiative forcing.

---

<sup>1</sup>Johnson Controls, NASA Ames Research Center, Moffett Field, California.

<sup>2</sup>Carnegie Institution of Washington, Department of Plant Biology, Stanford, California.

<sup>3</sup>NASA Ames Research Center, Moffett Field, California.

<sup>4</sup>Department of Biological Sciences, Stanford University, Stanford, California.

Most ecosystem-level understanding about the magnitude of CO<sub>2</sub> exchange with the terrestrial biosphere is based on correlations between measured fine-scale fluxes and climate characteristics [Friedlingstein et al. 1992; Raich and Schlesinger, 1992]. Satellite remote sensing can be used to extend this information; for example, the normalized difference vegetation index (NDVI) from the advanced very high resolution radiometer (AVHRR) has been used to estimate NPP and seasonal exchange of CO<sub>2</sub> between the atmosphere and the terrestrial biosphere [Tucker et al., 1986; Fung et al., 1987; Heimann and Keeling, 1989].

Many of the fundamental questions about the global carbon cycle can be addressed using simulation models that operate on a scale that links remote sensing, spatial data bases of climate and soils, and mechanistic understanding of atmosphere-plant-soil biogeochemistry. In this paper, we describe the development and application of the Carnegie-Ames-Stanford approach (CASA) Biosphere model for study of the terrestrial carbon cycle. Our overall objective was to characterize fixation and release of CO<sub>2</sub> using spatially (1° latitude-longitude) and temporally (monthly) resolved predictions of steady state net ecosystem production (NEP), the difference between NPP and R<sub>s</sub>.

**MODELING APPROACH**

The model runs on a monthly time interval to simulate seasonal patterns in net plant carbon fixation, biomass and nutrient allocation, litterfall, soil nitrogen mineralization, and CO<sub>2</sub> production. A

schematic representation of data input and ecosystem model integration is shown in Figure 1. Our fundamental approach was to define optimal metabolic rates for major ecosystem biogeochemical processes and to adjust these spatially uniform variables using unitless scalars related to the effects of air temperature, predicted soil moisture, litter substrate quality (N and lignin contents), soil texture, and land use. The coupled plant production and soil microbial respiration components of the model are regulated by a common soil moisture submodel. The model's NPP component is based on the concept of light-use efficiency explored by Monteith [1972, 1977]. The soil component simulates carbon and nitrogen cycling using a set of compartmental difference equations with a structure comparable to a somewhat simplified version of the CENTURY model [Parton et al., 1987, 1988]. Model input and state variables are stored as raster map arrays in a geographic information system (GIS). Major variables are defined in the appendix.

**GLOBAL DATA SETS**

All global data sets used as inputs to the model (Table 1) were resampled (if necessary) to a 1°x1° spatial resolution. Specific data sources are described in the following paragraphs.

*Vegetation Index*

We used monthly NDVI-FASIR (defined below) data sets for 1987 processed by Los et al. [1993] and Sellers et al. [1993]. This FASIR product includes a

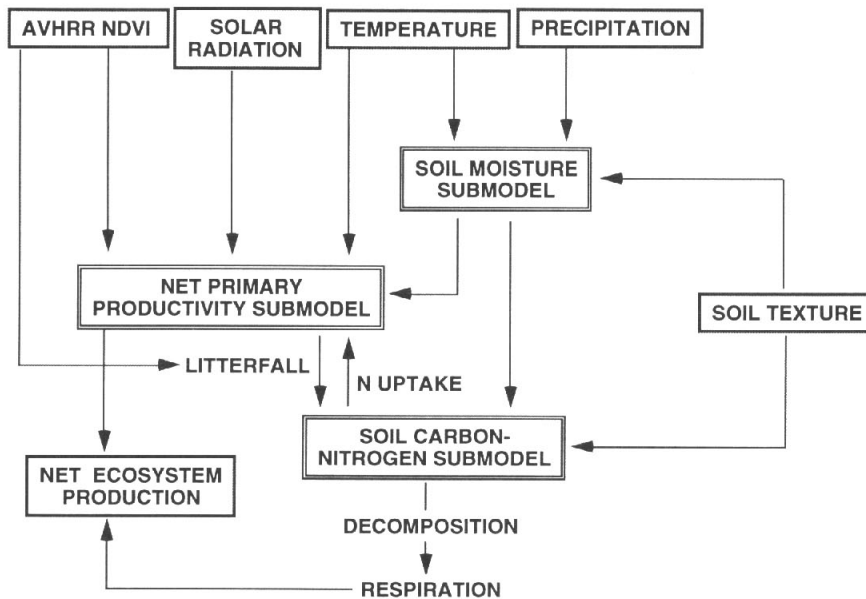


Fig. 1. Model integration framework. Global climate data sets are combined with soil texture settings to compute the monthly water balance, which controls NPP and soil microbial activity.

TABLE 1. Global Geographic Data Sets Used the Model

Name	Attributes	Source <sup>a</sup>	Resolution <sup>b</sup>	Reference
TEMP/PPT	Monthly temperature and precipitation	IIASA	0.5°x0.5°	Leemans and Cramer [1990]
SOLAR	Monthly 1987 solar radiation	GISS	5°x5°	Bishop and Rossow [1991]
NDVI	Monthly 1987 FAS/FASIR	GSFC	1°x1°	Los et al. [1993]
SIBVEG	Vegetation types	GSFC	1°x1°	Dorman and Sellers [1989]
GZTEX	FAO soil texture groups	GISS	1°x1°	Zobler [1986]
SOILC	Soil carbon densities	ARC/IIASA	0.5°x0.5°	Post et al. [1985] Leemans [1990]
SOILN	Soil nitrogen densities	ARC/IIASA	0.5°x0.5°	Post et al. [1985] Leemans [1990]

<sup>a</sup>Institutional sources of geographic data sets: ARC, NASA Ames Research Center, Moffett Field, California; GISS, NASA Goddard Institute for Space Studies, New York, New York; GSFC, NASA Goddard Space Flight Center, Greenbelt, Maryland; and IIASA, International Institute for Applied Systems Analysis, Laxenburg, Austria.

<sup>b</sup>Original resolution of gridded data.

Fourier adjustment (FA) to eliminate many effects of cloud contamination, a solar zenith angle correction (S), an interpolation (I) to prevent boreal forests from dropping to zero during winter months, and a reconstruction (R), in which all monthly values for evergreen tropical forests are held at the yearly maximum for those pixels. The reconstruction step eliminates further cloud interference that is characteristic of AVHRR-global area coverage (GAC) data for areas with frequent convective cloudiness. To identify the month of maximum NDVI and for estimation of the timing of litterfall, we used the FAS product which does not include I and R treatments.

#### Radiation

Solar radiation ( $W m^{-2} mo^{-1}$ ) data sets used in the model were computed surface irradiance from the International Satellite Cloud Climatology Project (ISCCP) [Bishop and Rossow, 1991]. They combine estimates of atmospheric optical depth from the ISCCP with calculations from a simplified general circulation model (GCM) transfer scheme to estimate monthly surface irradiance. These data have an accuracy of  $9 W m^{-2}$  on a daily basis and less than 4% bias in the 17-day mean relative to ground measurements.

#### Climate

The historical climate data sets we used were compiled by Leemans and Cramer [1990], who included stations with at least five years of

observations during period 1930-1960. Leemans and Cramer [1990] corrected the temperatures for altitude by combination of an estimated adiabatic lapse rate with global topographic coverage. The coverage quality of the data is considered best for Europe, North America, East Asia and Japan. We interpolated the data from Leemans and Cramer [1990] from their original  $0.5^{\circ} \times 0.5^{\circ}$  resolution to  $1^{\circ} \times 1^{\circ}$  using bi-directional splining.

#### Vegetation Characterization

We used the characterization of vegetation type from Dorman and Sellers [1989], modified as described in Sellers et al. [1993]. It is a simplified physiognomic classification based on the world vegetation classes of Kuchler [1983] and the land use database of Matthews [1984, 1985]. We use this classification system in the CASA model for two reasons: (1) It aggregates to a manageable number (12) of vegetation classes; and (2) Unlike other vegetation classification systems which are oriented toward ecologically based descriptions of the plant cover, the Dorman and Sellers [1989] classification is based on plant energy balance and life form dynamics, as these are most useful for coupling the land surface with atmospheric chemistry and physics. Areal extent and latitude zone distributions of the 12 vegetation classes are shown in Table 2.

#### Soil Type and Texture

Our model used the FAO/UNESCO [1971] Soil Map of the World (SMW) for characterization of soil

TABLE 2. Areas and Distributions of Global Vegetation Classes

Class	Description	n	Area, 10 <sup>6</sup> km <sup>2</sup>	%Land Cover	Latitude Zone Distribution (% Cover)				
					North, deg		South, deg		
					90-60	60-30	30-0	0-30	30-60
1	Broadleaf evergreen trees	1433	17.4	11.7	0	1	46	53	0
2	Broadleaf deciduous trees	258	2.3	1.5	0	75	14	0	11
3	Broadleaf and needleleaf trees	487	3.9	2.6	6	85	0	1	7
4	Needleleaf evergreen trees	2156	14.9	10.0	37	59	3	0	1
5	Needleleaf deciduous trees	1117	6.2	4.2	74	26	0	0	0
6	Broadleaf trees with groundcover	1582	18.2	12.2	1	14	27	55	3
7	Perennial grasslands	951	10.5	7.0	2	28	36	30	3
8	Broadleaf shrubs with grasslands	194	2.3	1.5	0	14	21	56	9
9	Broadleaf shrubs with bare soil	911	9.5	6.4	0	45	24	15	15
10	Tundra	1252	6.0	4.0	92	8	0	0	0
11	Bare soil and desert	1589	16.0	10.7	12	24	53	10	0
12	Cultivation	2783	26.4	17.7	0	67	15	6	12
13	Ice	7384	15.5	10.4					
Total		22097	149.0	100.0					

texture classes and their associated particle size distributions (Table 3). Data used to construct the SMW has been assembled from actual soil surveys (21% of global coverage); field reconnaissance of topography, geology, vegetation and climatic data (40% of global coverage); and general information from the local literature (39% of global coverage) [Gardiner, 1982]. Substantial disparities in the reliability of soil type classification have been identified over areas of tropical Central and South America and Africa [Gardiner, 1982; Richter and Babbar, 1991].

#### Soil Carbon and Nitrogen Contents

We created global gridded data sets by mapping Holdridge [1967] life zone soil C and N content ( $\text{g m}^{-3}$ ) averages reported by Post et al. [1985] to their corresponding life zone categories produced by Leemans [1990]. Spatial interpolation of the resulting data sets from  $0.5^\circ$  to  $1.0^\circ$  latitude/longitude was accomplished using bi-directional splining, preceded by nearest-neighbor fill to conserve land-water boundary elements. Soil profiles used in this data set were all from natural vegetation and excluded wetlands. Post et al. [1985] considered coverage of the original data to be best for tropical and cool temperate forests; coverage is poorer over extremely wet areas, dry tundra, dry boreal and warm desert life zones.

#### Other Variable Definitions

Ranges of certain other model variables were estimated from the literature, as discussed below.

These include leaf:root:wood C and N allocation ratios, litter and soil organic matter decomposition rates, and C assimilation efficiency of microbes. To simplify interpretations in this version of the model, we set spatially uniform values for most of these variables. As part of the modeling process, uniform rate constants related to photosynthesis and microbial respiration fluxes are adjusted for temporally and spatially resolved stress effects.

### MODEL STRUCTURE

#### Net Primary Productivity

New production of plant biomass (NPP) at a grid cell ( $x$ ) in month  $t$  is a product of intercepted photosynthetically active radiation (IPAR) and a light utilization efficiency ( $\epsilon$ ) that is modified by temperature and soil moisture (equation (1)). Neither IPAR nor  $\epsilon$  is dependent on ecosystem type.

$$\text{NPP}(x,t) = \text{IPAR}(x,t) \epsilon(x,t) \quad (1)$$

Monteith [1972, 1977] introduced models that estimate crop growth from IPAR. Subsequent empirical studies documented that  $\epsilon$  varies over a relatively narrow range for crop ecosystems (1.1 - 1.4  $\text{g C MJ}^{-1}$  PAR) but over a wider range for natural ecosystems [Russell et al., 1989]. Monteith's model incorporated the possibility of variation in  $\epsilon$  by making it a function of temperature, water, and nutrient stress.

IPAR is given by

TABLE 3. Soil Characteristics Estimated for FAO Texture Classes

Class	%Clay <sup>a</sup>	%Silt <sup>a</sup>	%Sand <sup>a</sup>	FC <sup>b</sup>	WP <sup>c</sup>	A <sup>d</sup>	B <sup>d</sup>	Soil C:N <sup>e</sup>
Coarse	9	8	83	0.51	0.20	0.002	-5.48	16
Coarse/medium	20	20	60	0.46	0.26	0.002	-6.54	14
Medium	30	33	37	0.60	0.34	0.013	-6.57	13
Medium/fine	48	25	27	0.65	0.43	0.006	-9.47	11
Fine	67	17	17	0.62	0.47	0.004	-13.78	10

Organic soils were assigned to the coarse/medium texture class [Bouwman et al., 1993].

<sup>a</sup>From Zabler [1986]

<sup>b</sup>Field capacity (m) for forested grid cells; FC(x) for other vegetation types are 50% of these values. Computed based on equation (2) in the work by Saxton et al. [1986] for soil water tension greater than or equal to 10 kPa. Tension was assumed to be 33 kPa for medium to fine textures and 10 kPa for coarse textures [Papendick and Campbell, 1980].

<sup>c</sup>Wilting point (m) for forested grid cells; WP(x) for other vegetation types are 50% of these values. Computed based on equation (2) in the work by Saxton et al. [1986] for soil water tension equal to 1500 kPa.

<sup>d</sup>From Saxton et al. [1986]; used in calculation of RDR.

<sup>e</sup>On the basis of weighted average particle-size C:N values reported by Anderson et al. [1981], Hinds and Lowe [1980], and Cameron and Posner [1979].

$$\text{IPAR}(x,t) = \text{SOL}(x,t) \text{FPAR}(x,t) 0.5 \quad (2)$$

where SOL is the total solar radiation incident on grid cell  $x$  in month  $t$ , from the database of Bishop and Rossow [1991], FPAR is the fraction of the incoming PAR intercepted by green vegetation, and the factor of 0.5 accounts for the fact that approximately half of the incoming solar radiation is in the PAR waveband (0.4–0.7  $\mu\text{m}$ ) [McCree, 1981].

FPAR is calculated as a linear function of the AVHRR simple ratio (SR), where

$$\text{SR}(x,t) = (1 + \text{NDVI}(x,t)) / (1 - \text{NDVI}(x,t)) \quad (3)$$

A linear relationship between FPAR and SR is supported by theoretical results from Kumar and Monteith [1981], Sellers [1985, 1987] Sellers et al. [1992] and Choudhury [1987], as well as from empirical studies [Demetriades-Shah et al., 1992a]. We used the SR-FPAR relationships developed by Sellers et al. [1993] to adjust slope and intercept terms in equation (4) for aggregate ecosystem groups.

$$\text{FPAR}(x,t) = \min\left\{\frac{\text{SR}(x,t) / [\text{SR}_{\max} - \text{SR}_{\min}]}{\text{SR}_{\min} / [\text{SR}_{\max} - \text{SR}_{\min}]}, 0.95\right\} \quad (4)$$

where  $\text{SR}_{\min}$  represents SR for unvegetated land areas and is set to 1.08 for all grid cells.  $\text{SR}_{\max}$  approximates the value at which all downwelling solar radiation is intercepted and corrects for effects of canopy architecture and residual cloud contamination.  $\text{SR}_{\max}$  was computed for four aggregate ecosystem groups according to the rationale of Sellers et al. [1993]. Using the 98th percentile of SR for ecosystem groups, vegetation classes 1 and 6 were set at 4.14; classes 2 and 3 at 6.17; 4 and 5 at 5.43; 7 through 12 at 5.13. A cap of 0.95 was imposed on FPAR in order to reflect a finite upper limit to leaf area.

The NPP formulation allows for regulation in either of the terms on the right side of equation (1). Several lines of evidence indicate that most of the regulation should be in IPAR, with less in  $\epsilon$ . One line of evidence comes from surveys which indicate that NPP of many ecosystem types is highly correlated with the annual integral of NDVI [Goward et al., 1985]. Another is the constancy of  $\epsilon$  from many experimental studies of unstressed plants, plus results from several studies indicating that nutrient stress [Garcia et al., 1988] and water stress [Squire et al., 1986] have much larger effects on IPAR than on  $\epsilon$ . Field [1991] considers ecological factors that should tend to constrain investments in light harvesting (which are manifested as IPAR) in relation to whatever resource or resources are limiting to growth so that all of the IPAR can be used for growth. A strong relationship between NPP and

IPAR does not necessarily indicate that light is the primary resource limiting to growth [Demetriades-Shah et al., 1992b].

Heimann and Keeling [1989] used a uniform  $\epsilon$  of 1.25 g C MJ<sup>-1</sup> PAR for a global light use efficiency model to calculate an annual terrestrial NPP of 56.4 Pg (10<sup>15</sup> g) C. With the solar radiation and NDVI data sets we used, this uniform  $\epsilon$  of 1.25 g C MJ<sup>-1</sup> PAR yields an annual global NPP of 185 Pg C yr<sup>-1</sup>, much above any recent estimates. Independent work suggests that  $\epsilon$  is not a universal constant [Russell et al., 1989]. To allow for effects of temperature and water stress on  $\epsilon$ , we calculate it as

$$\epsilon(x,t) = T_{\epsilon 1}(x,t) T_{\epsilon 2}(x,t) W_{\epsilon}(x,t) \epsilon^* \quad (5)$$

where  $T_{\epsilon 1}$  and  $T_{\epsilon 2}$  account for effects of temperature stress,  $W_{\epsilon}$  accounts for effects of water stress, and  $\epsilon^*$  is the maximum possible efficiency. The two temperature stress terms serve to depress  $\epsilon$  at very high and very low temperatures ( $T_{\epsilon 1}$ ) and to depress  $\epsilon$  when the temperature is above or below the optimum temperature ( $T_{\text{opt}}$ ), where  $T_{\text{opt}}(x)$  is defined as the air temperature in the month when the FAS NDVI reaches its maximum for the year (derived as shown in Plates 1a–1c).  $T_{\text{opt}}(x)$  ranges from near 0° C in the Arctic to the mid thirties in low latitude deserts.

$T_{\epsilon 1}(x)$ , which ranges from 0.8 at 0° C to 1.0 at 20° C to 0.8 at 40° C, is given by

$$T_{\epsilon 1}(x) = 0.8 + 0.02 T_{\text{opt}}(x) - 0.0005 (T_{\text{opt}}(x))^2 \quad (6)$$

For mean monthly temperatures of -10° C and below,  $T_{\epsilon 1}$  is set equal to zero. The basic motivation for including  $T_{\epsilon 1}$  is to reflect the empirical observation that plants in very cold habitats typically have low maximum growth rates [Chapin, 1980; Grime, 1979] and high root biomass [Sala et al., 1993], potentially imposing large respiratory costs. Plants in very hot environments may have high growth rates [Schulze and Chapin, 1987], but the efficiency of light utilization should be impacted by high rates of respiration [Amthor, 1989; Ryan, 1991].

Our  $T_{\epsilon 2}$  term, which reflects the concept that the efficiency of light utilization should be depressed when plants are growing at temperatures displaced from their optimum, has an asymmetric bell shape that falls off more quickly at high than at low temperatures. It is given by

$$T_{\epsilon 2}(x,t) = 1.1814 / \{1 + e^{[0.2 (T_{\text{opt}}(x) - 10 - T(x,t))]} / [1 + e^{[0.3 (-T_{\text{opt}}(x) - 10 + T(x,t))]}]\} \quad (7)$$

$T_{\epsilon 2}$  falls to half its value at  $T_{\text{opt}}$  at temperatures 10° C above or 13° C below  $T_{\text{opt}}$ . The idea behind

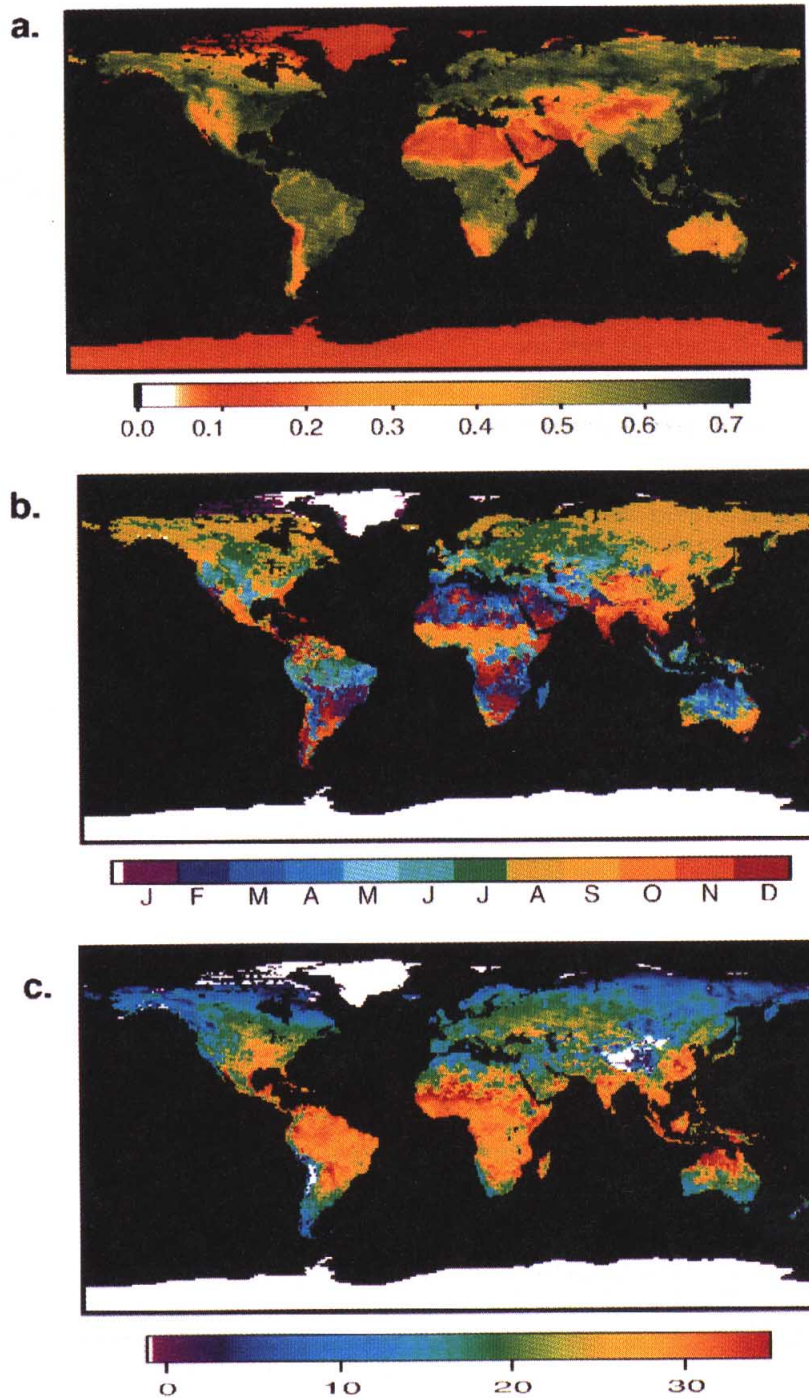


Plate 1. Results from the process of estimation of  $T_{opt}$ . (a) FAS-NDVI maximum for each grid cell during the model calibration year of 1987. (b) Month of the year when FAS-NDVI reached its maximum value. (c) Temperature ( $T_{opt}$ ) during the month of maximum FAS-NDVI; grid cells with  $T_{opt}$  less than  $-1^{\circ}\text{C}$  are shown in white.

including  $T_{e2}$  is to capture some of the intrinsic limitations on the flexibility of temperature acclimation. Adjusting  $T_{opt}$  to the temperature in the month of maximum NDVI assumes that plant growth is basically adapted to local ambient conditions, but  $T_{e2}$  reflects the fact that plant temperature responses cannot perfectly track ambient temperatures [Berry and Björkman, 1980].

The water stress factor ( $W_e$ ) is calculated as

$$W_e(x,t) = 0.5 + 0.5 EET(x,t)/PET(x,t) \quad (8)$$

where EET and PET come from the soil moisture submodel.  $W_e$  varies from 0.5 in very arid ecosystems to 1 in very wet ecosystems. For months when  $T$  less than or equal to  $0^\circ\text{C}$  and precipitation accumulates as snow pack on the surface, the  $W_e$  scalar value from the previous monthly time step is carried forward without change. It is similar in form to the water stress control on stomatal conductance in TEM [Raich et al., 1991], but it is less severe. We decreased the severity of the water stress impact on NPP to reflect the observation that most effects of water stress appear in IPAR rather than in  $\epsilon$  [Squire et al., 1986].

The maximum efficiency  $\epsilon^*$  is set through a single calibration using NPP observed at sites considered by Raich et al. [1991] and McGuire et al. [1992]. The calibration compares the annual observed NPP

( $NPP_{obs}$ ) with the annual NPP predicted ( $NPP_{pred}$ ) for the grid cell that includes each observation site. The  $\epsilon^*$  term is calculated through an iterative process that minimizes the following error function.

$$E = \sum_{x=1}^n [(NPP_{obs}(x) - NPP_{pred}(x))^2]^{0.5} / NPP_{pred}(x) \quad (9)$$

where  $n$  is 17 observation locations used for calibration and validation by Raich et al. [1991] and McGuire et al. [1992]. An initial estimate for the minimum  $E$  in equation (9) was obtained by calculating  $NPP_{pred}(x)$  values according to equations (1) and (5) with an  $\epsilon^*$  of  $0.405 \text{ g C MJ}^{-1} \text{ PAR}$ . This  $\epsilon^*$  value is consistent with a total terrestrial NPP of  $50 \text{ Pg C yr}^{-1}$ . The calibration is similar to calculating  $\epsilon^*$  such that the slope of a linear regression of  $NPP_{pred}$  versus  $NPP_{obs}$  approaches unity. It differs from that, however, in that the minimized term ( $E$ ) scales with the sum of the deviations divided by the predicted NPP, rather than simply the sum of the squared deviations. Division by  $NPP_{pred}$  in equation (9) makes the function sensitive to the proportional, rather than the absolute error in the fit. Because this calibration involves adjustment all the model grid cells by a constant factor, the correlation between model predicted and observed NPP is not affected by the error minimization process.

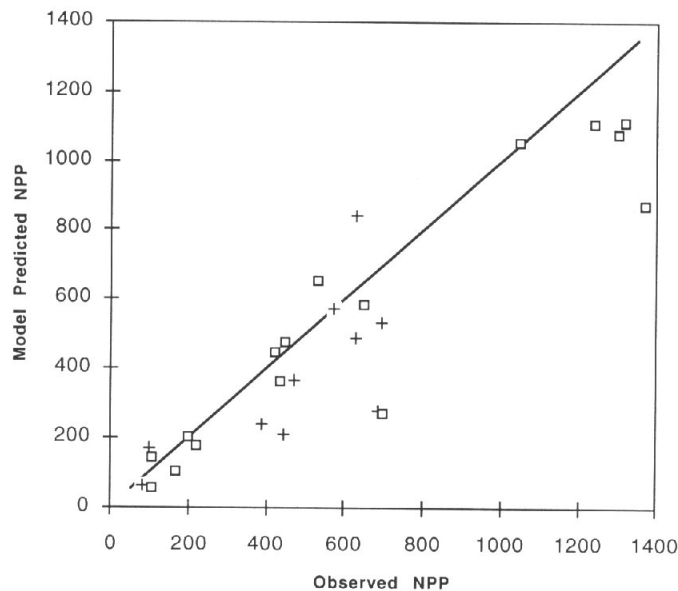


Fig. 2. Model predicted NPP for grid cells containing *in situ* NPP observations. Units are  $\text{g m}^{-2} \text{ yr}^{-1}$ . Site estimates marked with a box were used in a single step calibration to obtain  $\epsilon^*$ . These sites are the same as those used to calibrate and validate TEM [Raich et al., 1989; McGuire et al., 1992]. All TEM observational sites were used, with the exception of two (Taita, New Zealand and Guanica, Puerto Rico) that were not contained within land grid cells at a  $1^\circ \times 1^\circ$  resolution. The 1:1 regression line is shown for predicted versus observed values at TEM calibration sites. Validation sites marked with a plus were not used to calibrate  $\epsilon^*$ ; names and locations of these sites are listed in Table 4.

When  $E$  is minimized, the value of  $\epsilon^*$  is  $0.389 \text{ g C MJ}^{-1} \text{ PAR}$ . Predicted NPP values for the TEM sites cluster reasonably tightly around the 1:1 line ( $r^2$  of 0.89;  $p < 0.001$ ; Figure 2), with the exception of NPP for Chakia, India, a tropical deciduous forest for which McGuire et al. [1992] estimated root production using the carbon balance approach of Nadelhoffer and Raich [1992]. While our approach does a reasonable job of reproducing the measured NPP at the calibration sites, it is somewhat less satisfactory ( $r^2$  of 0.52;  $p < 0.01$ ) in prediction of NPP at several sites that were not used in calibrating the TEM (also shown in Figure 2 and listed in Table 4).

The motivation for this single step calibration is that we lack the understanding to estimate  $\epsilon^*$  from first principles. The maximum photon yield of photosynthesis sets an absolute upper bound on  $\epsilon^*$  of approximately  $2.88 \text{ g C MJ}^{-1} \text{ PAR}$  [Ehleringer and Björkman, 1977], but this value will always be reduced by saturation in the light response of photosynthesis. At the Harvard Forest, Wofsy et al. [1993] measured a gross primary productivity light use efficiency during summer months of around  $1.10 \text{ g C MJ}^{-1} \text{ PAR}$ . A 2:1 ratio of gross primary productivity to net primary productivity would argue for a maximum  $\epsilon^*$  of around  $0.55 \text{ g C MJ}^{-1} \text{ PAR}$  at Harvard Forest, fairly close to the  $\epsilon^*$  obtained through the above calibration.

#### Soil Moisture Submodel

Soil moisture content was calculated at each grid cell using monthly temperature and precipitation in combination with soil texture data and moisture-

holding capacity [Saxton et al., 1986]. This submodel is a one-layer "bucket" formulation that builds on previous simulation studies of regional and global surface hydrology [Mintz and Serafini, 1981; Vörösmarty et al., 1989; Bouwman et al., 1993].

Monthly soil moisture storage is calculated for each grid cell ( $x$ ) as a state variable, SOILM, with the potential to accumulate moisture over several months.

$$\text{SOILM}(x,t) = \text{SOILM}(x,t-1) - \begin{matrix} [\text{PET}(x,t) - \text{PPT}(x,t)] \text{ RDR} \\ \text{For } \text{PPT}(x,t) < \text{PET}(x,t) \end{matrix} \quad (10a)$$

$$\text{SOILM}(x,t) = \text{SOILM}(x,t-1) + \begin{matrix} [\text{PPT}(x,t) - \text{PET}(x,t)] \\ \text{For } \text{PPT}(x,t) \geq \text{PET}(x,t) \end{matrix} \quad (10b)$$

where PPT is average precipitation at month  $t$ , PET is potential evapotranspiration at month  $t$ , and RDR is a relative drying rate scalar for potential water extraction as a function of soil moisture (SOILM( $x,t-1$ )).

For months when temperature is less than or equal to  $0^\circ \text{C}$ , PET and PPT are set equal to zero and there is no net change in SOILM. During these months, precipitation accumulates as snow in a state variable PACK. PACK is added to PPT in the first month that monthly average air temperature ( $T$ )  $> 0^\circ \text{C}$ . This function initiates spring snow melt.

PET is calculated with the method of Thornthwaite [1948]. Lower and upper limits for SOILM were set at wilting point (WPT) and field capacity (FC), respectively (Table 3). These values were derived from soil texture relationships described by Saxton et

TABLE 4. NPP Model Validation Sites

Vegetation	Location	Latitude	Longitude	Reference
Desert shrub	San Simon, Arkansas	31° 50'N	109° 05'W	Chew and Chew [1965]
Grassland	Pantex, Texas	35° 18'N	101° 32'W	Sims and Coupland [1979]
Grassland	Cottonwood, South Dakota	43° 57'N	101° 52'W	Sims and Coupland [1979]
Savanna	Nairobi Park, Kenya	1° 20'S	36° 50'E	Kinyamario and Imbamba [1992]
Forest	Lubumbashi, Zaire	11° 29'S	27° 29'E	DeAngelis et al. [1981]
Oak forest	Oak Ridge, Tennessee	35° 55'N	80° 77'W	DeAngelis et al. [1981]
Forest	Hubbard Brook, New Hampshire	44° 00'N	71° 0'W	DeAngelis et al. [1981]
Forest	Solling, Germany	51° 49'N	9° 35' E	DeAngelis et al. [1981]
Forest-moss	BSMS, Alaska	64° 00'N	128° 00'W	DeAngelis et al. [1981]
Forest	Meathop, United Kingdom	54° 13'N	2° 53'W	DeAngelis et al. [1981]

These sites were chosen according to the following criteria: (1) Above and below ground NPP data were available. (2) Latitude and longitude coordinates of the site fell within land-designated model grid cells. (3) Sites were not near large metropolitan areas. (4) Sites were representative of the major ecosystems present within the grid cell.

al. [1986]. A matric potential of -10 kPa is used for calculating FC for coarse textured soils, whereas a -30 kPa potential is used for medium- to fine-textured soils [Papendick and Campbell, 1980].

The soil rooting depth for forests was set to 2.0 m. Grassland, tundra and cultivation classes (7, 10, and 12) were assigned a rooting depth of 1.0 m [Vörösmarty et al., 1989]. Several soil types were treated as special cases in assigning FC classes. Vertisols and ferrasols were assigned to the medium texture FC class, whereas andosols were assigned to the fine texture FC class [Bouwman et al., 1993]. Lithosols were assigned to a shallow soil class of 27% FC (total soil volume) with rooting depth of 0.1 m [Vörösmarty et al., 1989].

Additions to SOILM that exceed field capacity are assumed to leave the grid cell as runoff. There are no grid-cell interactions in the soil moisture submodel (i.e., runoff from one cell is not transferred to an adjacent cell).

Estimated evapotranspiration (EET) is calculated for each grid cell as

$$EET(x,t) = \min\{PPT(x,t)+[PET(x,t)-PPT(x,t)]RDR\}, \{PPT(x,t)+[SOILM(x,t-1)-WPT(x)]\}$$

For  $PPT(x,t) < PET(x,t)$  (11a)

$$EET(x,t) = PET(x,t)$$

For  $PPT(x,t) \geq PET(x,t)$  (11b)

Previous studies have shown that the rate of soil drying generally decreases with decreasing soil

moisture content and increasing soil water tension [Thornthwaite and Mather, 1957; Pierce, 1958; Pastor and Post, 1984]. We have fitted a family of logistic drying curves (Figure 3) for derivation of the RDR scalar using a transformation (equation (12)) of the relationship between soil water potential and volumetric moisture content presented by Saxton et al. [1986].

$$RDR = (1+a) / (1 + a \Theta^b) \tag{12}$$

where a and b are texture-dependent empirical coefficient and  $\Theta$  is the volumetric moisture content (m/m).

These curves resemble texture-dependent drying functions proposed previously [Holmes, 1961; Zahner, 1967]. Their forms imply that EET, a fraction of PET, is reduced dramatically for coarse and fine textured soils as  $\Theta$  falls below 0.4 and 0.8, respectively. For any month that PPT-PET is greater than zero, RDR is set to unity. When PET exceeds PPT, the potential loss of moisture from SOILM is adjusted by the RDR scalar, which is calculated according to the value of  $\Theta$  at t-1.

*Temperature and Moisture Effects on Microbial Respiration*

The effect of temperature on soil C and N fluxes ( $T_s$ ) was treated uniformly as an exponential ( $Q_{10}$ ) response (equation (13)) using a  $Q_{10}$  value of 2.0 [Fung et al., 1987; Anderson, 1991; Townsend et al., 1992].

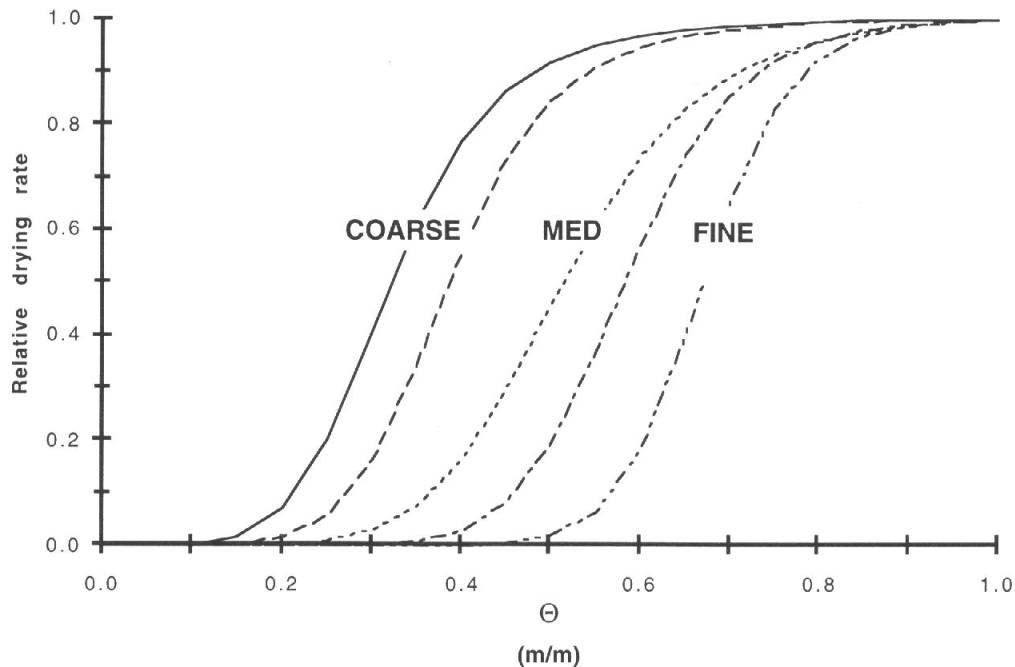


Fig. 3. Soil drying curves derived using a mathematical transformation equation (12) of the relationship between soil water potential and volumetric moisture content presented by Saxton et al. [1986].